On the Midlatitude Circulation in a High-Resolution Model of the North Atlantic

FRANK O. BRYAN

National Center for Atmospheric Research, Boulder, Colorado*

CLAUS W. BÖNING

Institut für Meereskunde an der Universität Kiel, Kiel, Germany

WILLIAM R. HOLLAND

National Center for Atmospheric Research, Boulder, Colorado

(Manuscript received 18 October 1993, in final form 14 March 1994)

ABSTRACT

This paper describes, and establishes the dynamical mechanisms responsible for, the large-scale, time-mean, midlatitude circulation in a high-resolution model of the North Atlantic basin. The model solution is compared with recently proposed transport schemes and interpretations of the dynamical balances operating in the subtropical gyre. In particular, the question of the degree to which Sverdrup balance holds for the subtropical gyre is addressed. At 25°N, thermohaline-driven bottom flows cause strong local departures from the Sverdrup solution for the vertically integrated meridional mass transport, but these nearly integrate to zero across the interior of the basin. In the northwestern region of the subtropical gyre, in the vicinity of the Gulf Stream, higher-order dynamics become important, and linear vorticity dynamics is unable to explain the model's vertically integrated transport. In the subpolar gyre, the model transport bears little resemblance to the Sverdrup prediction, and higher-order dynamics are important across the entire longitudinal extent of the basin.

The sensitivity of the model transport amplitudes, patterns, and dynamical balances are estimated by examining the solutions under a range of parameter choices and for four different wind stress forcing specifications. Taking into account a deficit of 7–10 Sv (Sv $\equiv 10^6$ m^3 s^{-1}) in the contribution of the model thermohaline circulation to the meridional transports at 25°N, the wind stress climatology of Isemer and Hasse appears to yield too strong of a circulation, while that derived from the NCAR Community Climate Model yields too weak of a circulation. The Hellerman and Rosenstein and ECMWF climatologies result in wind-driven transports close to observational estimates at 25°N. The range between cases for the annual mean southward transport in the interior above 1000 m is 14 Sv, which is 40%–70% of the mean transport itself. There is little sensitivity to the model closure parameters at this latitude. At 55°N, in the subpolar gyre, there is little sensitivity of the model solution to the choice of either closure parameters or wind climatology, despite large differences in the Sverdrup transports implied by the different wind stress datasets. Large year to year variability of the meridional transport east of the Bahamas makes it difficult to provide robust estimates of the sensitivity of the Antilles and deep western boundary current systems to forcing and parameter changes.

1. Introduction

In this study we use the high-resolution model of the North Atlantic developed under the World Ocean Circulation Experiment (WOCE) Community Modeling Effort (CME) to investigate the distribution of mass transport and the dynamical processes operating in the subtropical gyre. A question of particular interest is how do the primarily horizontal, wind-driven circulation and the thermohaline-driven, meridional overturning circulation interact in producing the observed meridional transports of the Florida Current and the western boundary current system to the east of the Bahamas.

A closely related issue is the degree to which Sverdrup balance is able to describe the local and basin-integrated meridional volume transports. The simplest expression of Sverdrup balance follows from the vertically integrated, steady, linear, inviscid vorticity balance

$$\beta V_g = f w_s - f w_b, \tag{1}$$

where V_g is the vertically integrated geostrophic transport, w_s is the vertical velocity at the base of the surface Ekman layer, and w_b is the vertical velocity at the bottom. In the case that the vertical velocity at the bottom is small relative to that at the surface, we have

* The National Center for Atmospheric Research is sponsored by the National Science Foundation.

Corresponding author address: Dr. Frank O. Bryan, National Center for Atmospheric Research, P.O. Box 3000, Boulder, CO 80307.

$$\beta V_g = f w_s = f \mathbf{k} \cdot \nabla \times \frac{\boldsymbol{\tau}}{f}, \tag{2}$$

or equivalently,

$$\beta V = \mathbf{k} \cdot \nabla \times \boldsymbol{\tau}, \tag{3}$$

where the total meridional transport V is the sum of the geostrophic transport V_g and the meridional transport in the surface Ekman layer $-\tau^x/f$.

The applicability of Eq. (2) or (3) to the North Atlantic is under debate, since the oceanic database does not support direct estimates of the individual terms in the vorticity equation. In the case of a purely wind-driven ocean, baroclinic compensation of the surface pressure field leads to vanishing deep flow and establishes Sverdrup balance as illustrated in the model studies of Anderson and Killworth (1977) and Anderson et al. (1979). However, as noted by Wunsch and Roemmich (1985), there is little reason to expect Sverdrup balance to hold in reality, where the interaction of the deep flow associated with the thermohaline-driven circulation and the bottom topography can lead to nonnegligible bottom pressure torque fw_b. Holland (1973) provided a numerical example of this latter effect in the context of a basin with idealized geometry, topography, and forcing.

Nevertheless, a number of diagnostic studies have suggested that Eq. (2) may provide an adequate description of the meridional transport of the subtropical gyre in the North Atlantic. Figure 1, adapted from Roemmich and Wunsch (1985), shows the geostrophic transport above $\sigma_\theta = 27.4$ along 24.5°N to be in fair agreement with the transport predicted by Eq. (2) for that latitude, at least for the eastern two-thirds of the basin. Interpretations of this partial agreement differ widely, however. Leetmaa et al. (1977) attribute the discrepancies in the western third of the basin to "low frequency eddies" and "higher-order dynamics." By extrapolating transport per unit width from the interior, they estimate the total southward transport between the African continent and the Bahamas as 30 Sv (Sv $\equiv 10^6$ m^3 s^{-1}). Since this value is equal to the measured northward transport in the Straits of Florida (Larsen 1992), the authors suggested a mass conserving circulation scheme consisting of a primarily horizontal wind-driven circulation in the upper ocean, with the northward transport in the Straits of Florida completely supplied by southward Sverdrup transport in the interior.

However, as pointed out by Roemmich and Wunsch (1985) and Wunsch and Roemmich (1985), this view of the meridional transport is inconsistent with the existence of a meridional overturning cell associated with the formation and export to the South Atlantic of North Atlantic Deep Water (NADW). Estimates based on hydrographic section data along 24.5°N (Hall and Bryden 1982; Roemmich 1980; Roemmich and Wunsch 1985) suggest a southward transport of 14–17 Sv below 1000-m depth. A recent study by Schmitz and Richardson (1991), using water mass analysis techniques, identified 13 Sv of the flow through the Straits of Florida as water of South Atlantic origin, that is, as a component of the large-scale thermohaline overturning cell. According to this view, the subtropical gyre contributes only about 17 Sv to the transport in the Florida Current. Schmitz et al. (1992) suggested that this wind-driven component is derived from the southward Sverdrup transport across 25°N to the east of 55°–60°W.

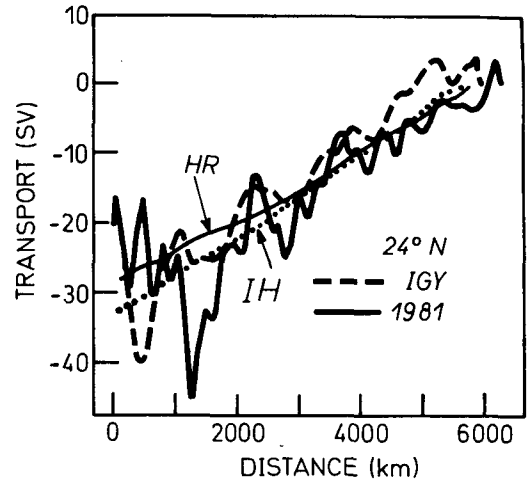

FIG. 1. Comparison of the geostrophic transport relative to $\sigma_\theta = 27.4$ for two hydrographic surveys, and the Sverdrup transport predicted by Eq. (2) for the Hellerman–Rosenstein and Isemer–Hasse wind stress distributions. [Adapted from Roemmich and Wunsch (1985)].

The nature of the observed circulation between 60°W and the Bahamas is much less certain. Figure 1 indicates the presence of energetic flows on smaller horizontal scales varying between the times of the two hydrographic surveys. Part of this structure could be associated with the recirculation regime of the Gulf Stream, thus involving higher-order dynamics (Roemmich and Wunsch 1985). Alternatively, Schmitz et al. (1992) noted a similarity between the dynamic height contours in the region and the transport contours computed from Eq. (2). Several studies of the local upper-layer circulation to the east of the Bahamas have addressed the question of the existence and structure of the Antilles Current. In the inverse model analysis of Roemmich and Wunsch (1985) there is a northward transport of 10 Sv, difficult to reconcile with the weak flow of less than 4 Sv obtained by Olson et al. (1984) using regional hydrography and current meter data. Direct current meter measurements to the east of Abaco Island at 26.5°N show strong variability of the boundary current system on timescales of about 100 days, making the determination of a long-term mean a difficult task. Recent estimates of the transport by Lee et al. (1990) based on long-term current meter moorings give a northward transport in the upper 800

m of 3.2 ± 7.6 Sv. Subsequent mooring deployments in the same area indicate even greater variability in the upper-layer transport: 7.1 ± 8.8 Sv and 3.9 ± 9.6 Sv (E. Fillenbaum 1993, personal communication).

In addition to the difficulties associated with determining the absolute transport across the section from oceanographic data, there remain considerable uncertainties in the estimates of the wind stress. Previous calculations of the wind-driven transport in the North Atlantic, including Leetmaa et al. (1977) and Roemmich and Wunsch (1985), have relied on wind stress climatologies derived from historical marine meteorological observations and bulk aerodynamic parameterizations developed by Bunker (1976); the most widely used being the climatology of Hellerman and Rosenstein (1983) (hereafter HR). In recent years there has been growing concern about possible systematic errors in these derivations. Measurements and theoretical results indicated significantly lower values for the drag coefficient under open-ocean conditions than had been used by Bunker (1976) or HR. Harrison (1989) computed monthly mean wind stress values from a dataset similar to that used by HR (1983), but with the drag coefficient specification of Large and Pond (1981), obtaining stresses that were about 20% smaller. Isemer and Hasse (1987, hereafter IH) presented a climatology for the North Atlantic with revised parameterizations for both the drag coefficient and the Beaufort scale to wind speed conversion. The IH stresses are significantly higher than those of HR for the trade wind region. The nearly 100% difference in magnitude between the stresses of IH and Harrison (1989) for that region illustrates the current uncertainty of wind stress estimates based on marine meteorological observations (Böning et al. 1991a). In Fig. 1, estimates of the Sverdrup transport based on both the HR and IH climatologies are shown. The differences between the two estimates are small in the eastern half of the basin, but grow to about 7 Sv near the western boundary. Both estimates of the Sverdrup transport agree reasonably well with the observed geostrophic transports in the eastern 4000 km; in fact, the section data would not allow the rejection of either wind stress climatology.

In this study we use the results from a set of experiments with the CME North Atlantic Model to explore the issues described above. The experiments cover a range of parameter space and wind stress specifications (Table 1). Aspects of some of these experiments have been described in previous papers. Böning et al. (1991b) examined seasonal and subseasonal variability of transport in the western boundary current of the subtropical gyre. Treguier (1992), Stammer and Böning (1992), and Beckman et al. (1994) discuss mesoscale variability and energetics. Spall (1990, 1992) described the mean flow and variability in the upper layers of the eastern subtropical gyre. The sensitivity of the circulation in the tropical region to the choice of wind stress climatology is described in Bryan et al. (1994). This study builds on these previous analyses and furthers the original goal of the CME: to evaluate the performance of state of the art general circulation models through direct comparison with observations. Our focus in this paper is on the long-term mean and low-frequency variability of the horizontal mass transport in the midlatitude North Atlantic. Two companion papers (Böning et al. 1994, 1995) address the primarily thermohaline-driven meridional circulation and the poleward heat transport of the model solution. In section 3 we describe the three-dimensional structure of the time-mean circulation with particular attention to the region of the subtropical gyre centered on 25°N. In the following sections, vertically integrated mass transports and the distribution of transport with depth and temperature classes along several latitude circles are presented and compared with observational estimates. In section 6, we examine the degree to which the model-predicted transport can be explained by linear vorticity dynamics.

2. Model description and experiment design

The basic model used in these experiments is the primitive equation model developed at the NOAA Geophysical Fluid Dynamics Laboratory by Bryan (1969) and Cox (1984). The particular configuration used here is based on the model developed for the WOCE CME and has been described in Bryan and Holland (1989). The horizontal resolution is 1/3° in latitude and 2/5° in longitude. There are 30 discrete levels in the vertical, with a spacing of 35 m at the surface and smoothly stretching to 250 m by 1000 m depth. Below 1000 m the vertical grid spacing is a constant 250 m. The computational domain is the Atlantic basin from 15°S to 65°N latitude, including the Caribbean Sea and Gulf of Mexico, but excluding the Mediterranean Sea. Cuba and Hispañola are treated as true islands, smaller islands being represented as shallow seamounts or shoals. Bottom topography is represented in the model as stacked grid boxes, so that the bottom lies on the interface between two grid levels. The topography is derived from a digital terrain dataset with 5′ latitude–longitude resolution using a simple nearest neighbor approach. The only smoothing performed is to remove single gridpoint holes or spikes.

The horizontal dissipation mechanism for both momentum and tracers is a highly scale-selective, biharmonic operator. The vertical dissipation mechanism is the more traditional second-order operator with constant coefficients. The coefficients used in each of the experiments described in this paper are listed in Table 1. Additional dissipation of momentum is effected by a quadratic bottom drag. A conventional adjustment scheme is used to treat free convective mixing.

The surface boundary conditions are all based on seasonal climatological datasets. The surface thermal

TABLE 1. Summary of experiment configurations. Integration period is the length of the experiment in years, analysis period is the number of years (at the end of the experiment) used in computing statistics presented in this paper. See text for discussion of wind stress acronyms. (*) Experiment K13-5 used daily wind stress anomalies for the year 1986 from ECMWF superimposed on the IH annual mean. A_{MH} is horizontal hyperviscosity, A_{HH} is horizontal hyperdiffusivity, A_{MV} is vertical viscosity, and A_{HV} is vertical diffusivity.

Experiment	Initial condition	Integration period	Analysis period	Wind data	A_{MH} ($cm^4\ s^{-1}$)	A_{HH} ($cm^4\ s^{-1}$)	A_{MV} ($cm^2\ s^{-1}$)	A_{HV} ($cm^2\ s^{-1}$)
N13-1	Levitus	25	15	HR	-2.5×10^{19}	-2.5×10^{19}	30	0.3
N13-2	N13-1 at year 20	5	5	HR	-1.0×10^{19}	-2.5×10^{19}	10	0.3
N13-3	N13-2 at year 21	5	5	ECMWF	-1.0×10^{19}	-2.5×10^{19}	10	0.3
N13-4	N13-2 at year 21	5	5	CCM2	-1.0×10^{19}	-2.5×10^{19}	10	0.3
K13-1	N13-1 at year 16	8	5	HR	-2.5×10^{19}	-2.5×10^{19}	10	0.3
K13-2	K13-1 at year 20	8	5	IH	-2.5×10^{19}	-2.5×10^{19}	10	0.3
K13-3	K13-2 at year 20	4	4	IH	-0.8×10^{19}	-2.4×10^{19}	10	0.3
K13-5	K13-4 at year 28	5	5	IH*	-2.5×10^{19}	-2.5×10^{19}	10	0.3

boundary conditions are specified by a linear bulk formula described by Han (1984). In this scheme the heat flux is a linear function of the difference between the model-predicted, sea surface temperature and a prescribed "effective," atmospheric temperature. The proportionality coefficient varies temporally and spatially in the range 25–60 $Wm^{-2}\ K^{-1}$, and is primarily a function of surface wind speed. Due to the lack of reliable datasets for precipitation over the ocean, the surface boundary condition for freshwater flux is implemented as a linear damping of salinity in the first model level toward the Levitus (1982) seasonal climatology.

Four different wind stress climatologies have been used to force the model as shown in Table 1. The original data for each are provided at different resolutions and in somewhat different form, so the procedure for transfer to the model grid will be briefly described for each case.

The Hellerman and Rosenstein (1983) climatology is provided on a 2° lat. × 2° long. grid. Monthly mean wind stress values are provided uniformly over the globe, including land areas (presumably filled in by their objective analysis procedure). These values are interpolated to the ocean model grid using bicubic splines. The choice of cubic over linear interpolation is motivated by the desire to maintain smoothly varying derivatives, for example, the curl of the wind stress. Since the resolution of the model grid is considerably higher than that of any of the wind stress datasets, a linear interpolation would yield a constant curl over several adjacent model points, and then a jump to a new value.

The Trenberth et al. (1990) dataset (hereafter ECMWF) is based on twice daily synoptic analyses of 1000-mb winds for the period 1980–1986. The synoptic maps of wind stress are averaged into ensemble monthly means for this period. Wind stress values are provided uniformly over the globe on a 2.5° lat × 2.5° long grid. As in the HR case, the monthly mean values are interpolated to the ocean model grid using bicubic splines.

The Isemer–Hasse wind stress climatology has been thoroughly described in Böning et al. (1991a). It represents a version of the Bunker Atlas for the North Atlantic based on revised parameterizations as discussed above. In contrast to the other datasets, the IH climatology extends only to the equator. For cases indicated as being driven by the IH wind stress, the HR stresses are used in the Southern Hemisphere with a smooth transition between the two climatologies over a 5° latitude band north of the equator.

The NCAR CCM2-based climatology (hereafter CCM2) is derived from a 10-year control integration of the NCAR Community Climate Model (Hack et al. 1993) driven by climatological, monthly mean sea surface temperatures. Transfer of the wind stress to the ocean model grid is treated somewhat differently for this dataset. Due to a discontinuity in the surface roughness parameter between land and ocean, there are very large changes in the wind stress at the coastlines. Interpolating wind stress (or any other surface flux quantity) from the CCM2 grid to the ocean model grid, using the same procedure as described above, introduced spurious edge effects that had a particularly deleterious impact on the wind stress curl field. To ameliorate this problem, daily averages of each surface level atmospheric state variable (and the SST field originally used to drive the CCM) were individually interpolated from the CCM T42 transform grid (approximately 2.8° horizontal resolution) to the ocean model grid using bicubic splines. The wind stress was recomputed using the interpolated state variables and the same bulk formula used by the atmospheric model, at the ocean model resolution. The resulting wind stress field was essentially identical to the original atmospheric model result over open ocean areas but with considerably reduced errors near coastlines. These daily maps for a 10-year period were then averaged into ensemble monthly means.

In all cases (except K13-5, where daily values were used), the monthly mean wind stress values were treated as midmonth values and the stress was linearly interpolated to the model simulation time at each time

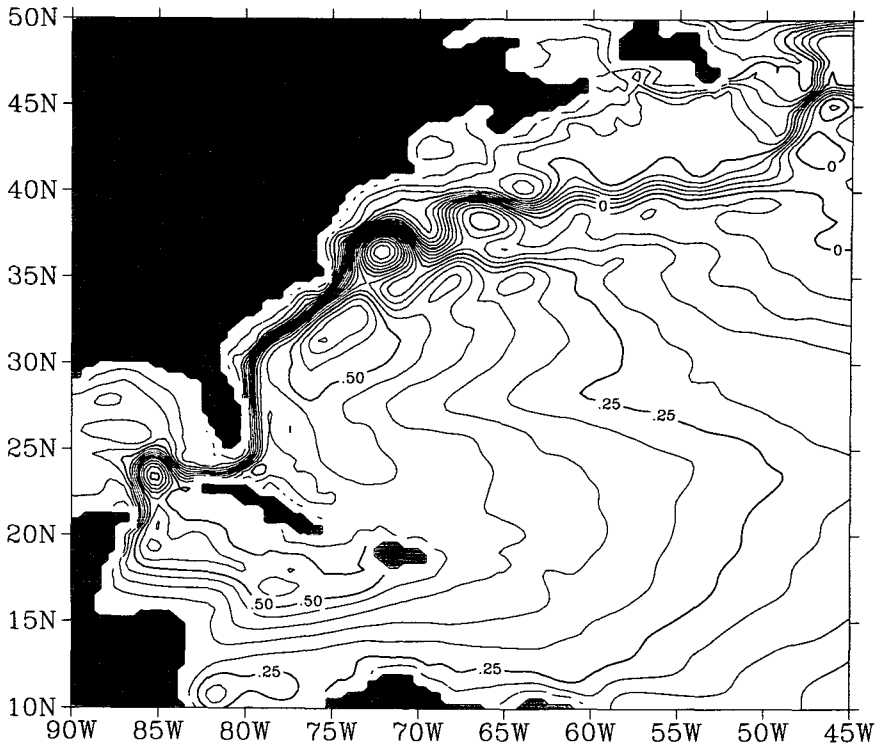

FIG. 2. Climatological-mean surface pressure distribution in the southwestern subtropical gyre for case N13-2. Contour interval is 0.05 decibars, or equivalently 5 cm.

step. Note that the linear time interpolation procedure can cause the monthly mean stress actually felt by the ocean model to have slightly lower amplitude than the monthly mean data itself.

The restriction of the model domain to a less than global one decreases the computational burden considerably, but introduces the complication of open boundaries. In these experiments the boundaries are closed to inflow or outflow, but narrow "buffer zones" are introduced adjacent to them. In these buffer zones the temperature and salinity are damped toward their (seasonally varying) climatological values on a timescale of 25 days at the outer edge (approximately 150 km from the walls), linearly decreasing to 5 days adjacent to the wall. The damping terms in these buffer zones must provide the heat and salt sources and sinks, for example, to convert southward flowing NADW to northward flowing surface waters at the southern boundary. The efficiency and accuracy of this conversion process thus control, to a large extent, the strength of the thermohaline circulation in the model. Similar buffer zones are introduced near Gibralter to provide the influence of Mediterranean water mass, and in a region along the northwestern boundary of the Labrador Sea. A subsequent paper (Böning et al. 1994) will address the success of the buffer zone approach as well as the sensitivity of the model results to the parameter values and data used in the buffer zone forcing.

The initial condition and integration period for each experiment are shown in Table 1. All except the first NCAR experiment are initialized with a solution from a previous experiment. The analysis period shown in Table 1 indicates the period over which the means shown in subsequent sections were computed. Monthly, annual, ensemble monthly, and ensemble annual means are computed from snapshots of the solution recorded approximately every 3 days (10 samples per month).

3. The time-mean, large-scale circulation

As the three-dimensional circulation in the model is extremely complex, providing a thorough description of the flow field and hydrography is beyond the scope of any one paper. In this section we will briefly describe those aspects of the flow that are primarily involved in the large-scale horizontal mass transport. We also focus on flow features that strongly interact with the topography. The results presented in this section are for case N13-2. While there are quantitative differences between cases, as described below, the large-scale features of the time-mean circulation are qualitatively similar for all cases considered in this paper.

The surface pressure field in the southwest quadrant of the subtropical gyre for case N13-2 is shown in Fig. 2. A feature of particular note is the trough along 27°N

west of 60°W. This results in a C-shaped pattern that has been noted previously in several observational estimates of dynamic height in the region (Schmitz et al. 1992) and also appears in the estimates of Sverdrup transport obtained from Eq. (2) (Böning et al. 1991a).

The transport in the layer above 7°C [the boundary between warm and cold waters used by Schmitz and McCartney (1993)] is shown in Fig. 3. As noted by Schott and Böning (1991), it is difficult to identify a direct boundary current link between the Southern Hemisphere and the Carribean for this layer. The primary source for water passing through the Lesser Antilles is zonal flow from the interior. In his examination of the circulation east of 40°W, Spall (1990) noted a significant contribution of waters of South Atlantic origin to the hydrographic structure in the model solution for that region. Thus, a more indirect route is indicated. Spall (1990) established that the model predictions of upper-ocean current positions and transports for the eastern basin were generally in good agreement with observations. In particular, the model prediction of approximately 11 Sv southward transport across 25°N above 800 m, east of 40°W, is in good agreement with the estimate of Stramma (1984).

In addition to the flow entering through the passages of the Lesser Antilles, there is significant inflow to the Caribbean through Anegada Passage east of the submerged representation of Puerto Rico, Mona Passage between Puerto Rico and Hispañola, and Windward Passage between Cuba and Hispañola. In each case the strength of the flow in the passage is enhanced relative to the background flow in the immediate region. While northward flow along the Antilles Arc is apparent as far south as 17°N, the main formation region of the Antilles Current is near 22°N. The larger fraction of the northward transport across 25°N (discussed in more detail below) passes through the Straits of Florida, with virtually all of the Florida Current transport having passed through the Caribbean and Gulf of Mexico. The transports through the model representations of

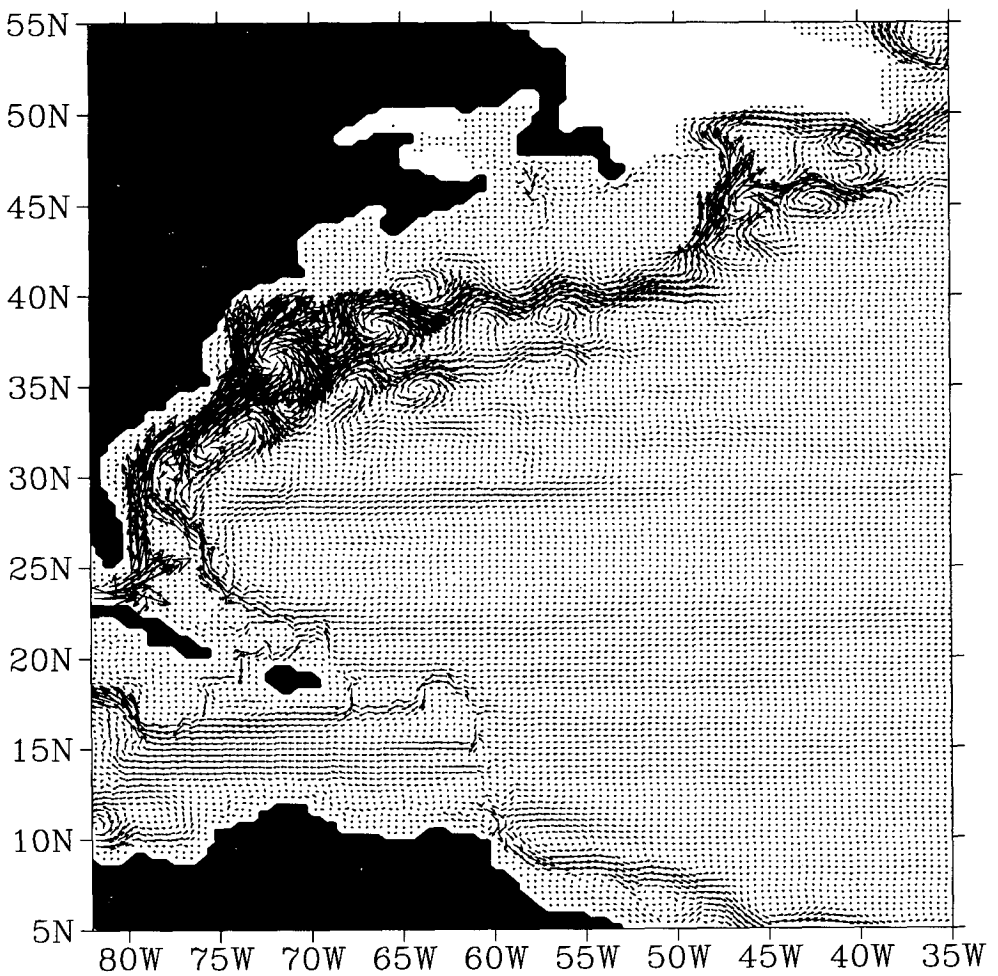

FIG. 3. Vertically integrated climatological-mean horizontal velocity between the surface and the 7°C isotherm in the western subtropical gyre. A vector 5° longitude in length represents a vertically integrated velocity of 6×10^6 cm^2 s^{-1}.

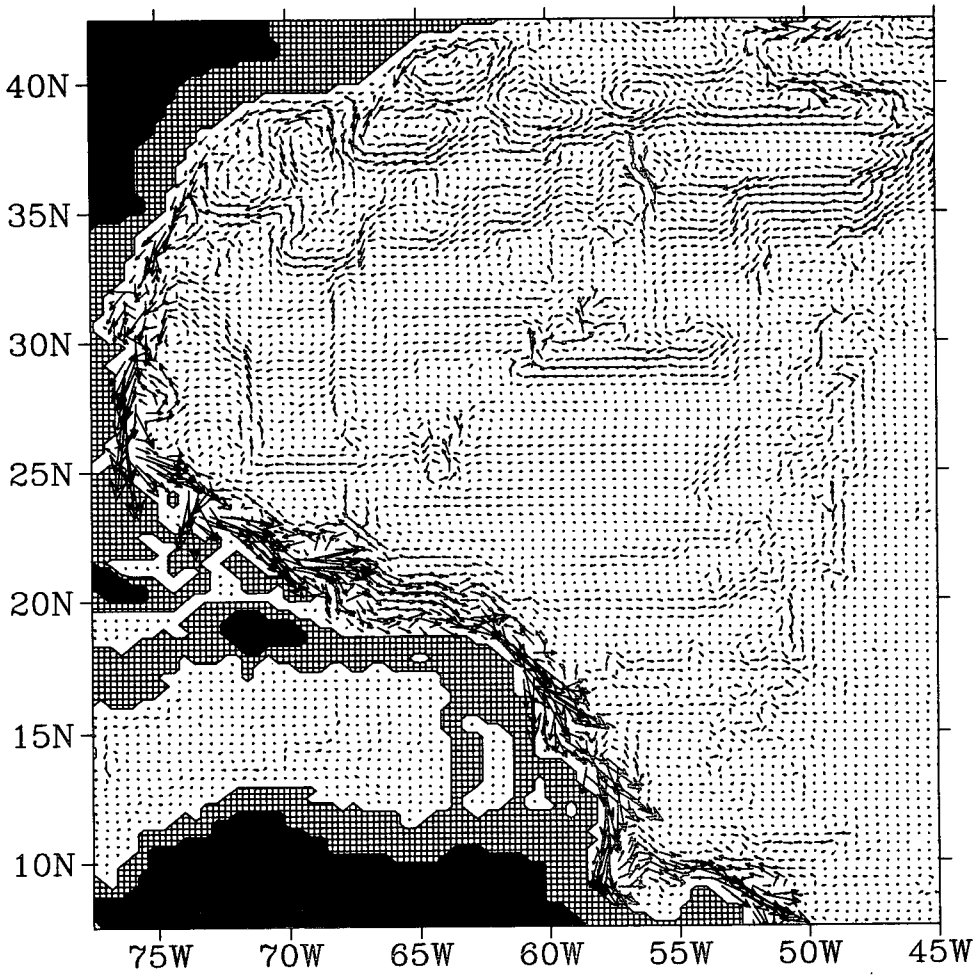

FIG. 4. Vertically averaged climatological-mean horizontal velocity between 2000 and 3000 m in the western subtropical gyre. Topography shallower than 2000 m is crosshatched. A vector 5° of longitude in length represents a velocity of 15 cm s^{-1}.

the Old Bahama Passage and New Providence Channel are negligible.

The transport in the boundary current increases downstream from the Straits of Florida, but not as strongly as in observations. The zonal jet associated with the trough seen in the dynamic height field in Fig. 2 contributes about 5 Sv to the boundary current transport. The transport passing Cape Hatteras in the layer warmer than 7°C is approximately 40 Sv, compared to observational estimates around 55 Sv (Schmitz and McCartney 1993). After separation from the coast, the Gulf Stream has several quasi-standing meanders that diminish in amplitude with distance offshore. There is some indication of a split jet or bimodal positioning of the jet, with a weaker southern branch between 35°N and 37°N, the stronger branch around 40°N. The transport in the separated jet diminishes downstream to values that are significantly lower than observed. At 60°W, the upper-layer eastward transport north of 35°N is 29 Sv and decreases to 25 Sv at 50°W. By comparison, the transport scheme of Schmitz and McCartney (1993) has an upper-layer transport in the Gulf Stream of 55 Sv at 50°W. At least part of this deficit can be attributed to the lack of a cyclonic recirculation gyre north of the Gulf Stream in the model. As the Gulf Stream in the model passes 50°W, it reattaches to the boundary and intensifies. A second separation occurs to the east of the Grand Banks. Again, the separated jet shows a split structure with cores near 46°N, south of Flemish Cap, and along the outcrop for this layer near 50°N.

The southward transport of NADW is shown in Fig. 4. A coherent boundary current exists from 35°N down to the southern boundary of the model. North and east of Cape Hatteras there is weak westward flow along the boundary, but the strongest flow occurs in a complicated set of recirculations under the Gulf Stream. Some of the smaller-scale features such as the merid-

ional flows along 50°W reflect the bottom topography below this layer.

The deepest layers of the model (Fig. 5) are dominated by the circulation of Antarctic Bottom Water (AABW). There is a net transport of 5 Sv of AABW across the equator. The separation from the western boundary and transport along the eastern flank of the Bermuda Rise is consistent with the schematic transport pattern of Schmitz and McCartney (1993). More detailed discussion of the distribution and transports of deep water masses is provided in Böning et al. (1994).

In section 5 we provide a detailed examination of the mass balance along 25°N. In Fig. 6 we show the structure of the meridional velocity along this section. Böning et al. (1991b) provide a detailed description of the boundary current structure for this latitude. With only three grid points across the Straits of Florida, it is difficult to resolve the asymmetries in the velocity field and topography of the actual straits. The Antilles Current has a subsurface maximum at 300 m, of approximately 25 cm s^{-1}, with mean northward flow extending to 1500 m. The maximum velocity and vertical structure are in good agreement with the Pegasus-referenced geostrophic velocity sections at 26.5°N presented in Lee et al. (1990) and Leaman and Harris (1990). The southward recirculation offshore has less vertical shear and eventually merges with the southward transport of North Atlantic Deep Water. The velocity core of the deep western boundary current occurs at 1750 m with maximum velocities near 4 cm s^{-1}. This is 750–1000 m shallower than the observed velocity core (Lee et al. 1990), and a factor of 4 to 5 weaker. The velocity maximum in the model's deep western boundary current also occurs farther offshore than is observed. The northward transport of AABW occurs below and offshore of the southward flowing NADW. Note that much of the AABW separates from

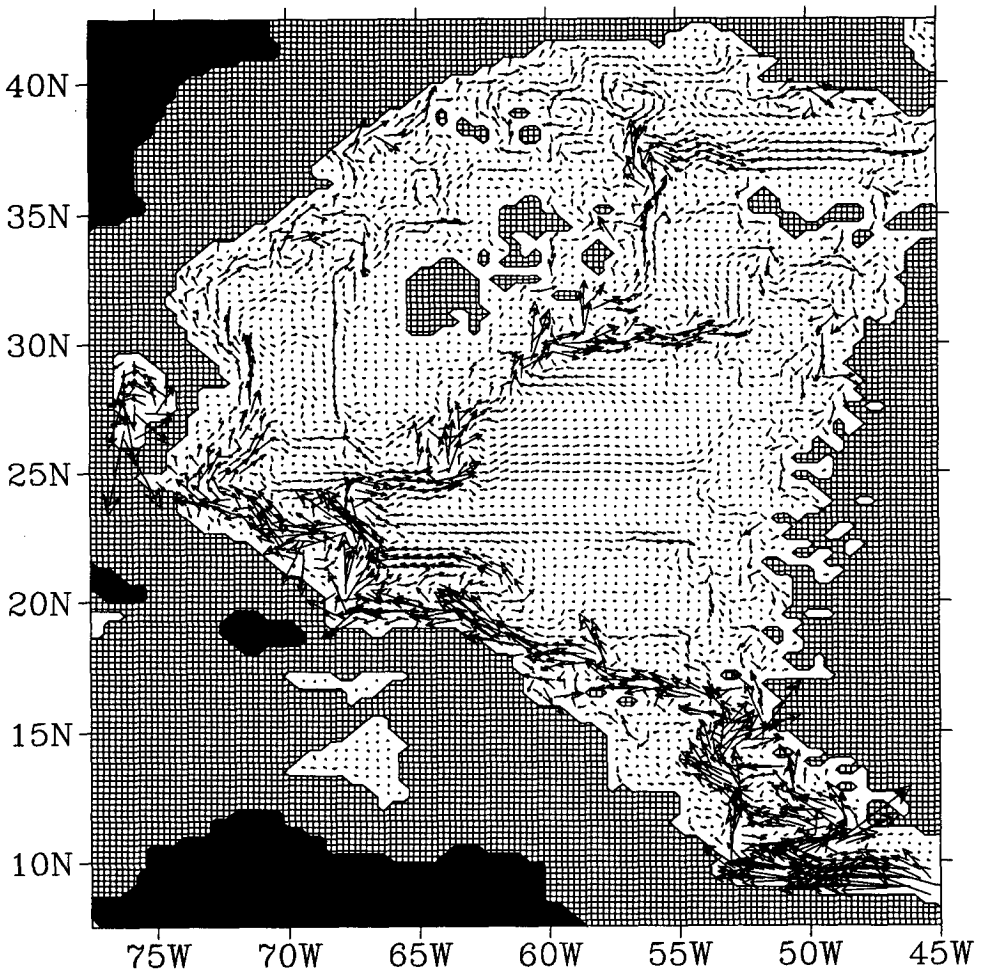

FIG. 5. Vertically averaged climatological-mean horizontal velocity between 4500 and 5500 m in the western subtropical gyre. Topography shallower than 4500 m is crosshatched. A vector 5° of longitude in length represents a velocity of 10 cm s^{-1}.

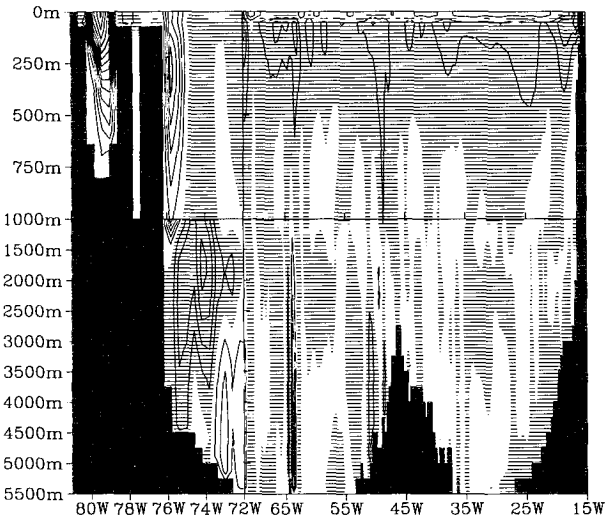

FIG. 6. Meridional component of the climatological-mean velocity along 25°N. Southward velocities are indicated by hatching. The horizontal scale is expanded west of 72°W, and the vertical scale is expanded above 1000 m. The contour interval is 5 cm s^{-1} above 1000 m and west of 72°W, and 1 cm s^{-1} elsewhere.

the western boundary south of 25°N, however. In the interior we can distinguish two flow regimes. The upper 500–1000 m are characterized by broad zonal scales of the baroclinic fields. The deeper ocean is characterized by shorter zonal scales and locally intensified flows near steep topography. The strong meridional velocities near 65°W, for example, are associated with flow around the southern tip of the Bermuda rise.

4. Vertically integrated mass transport

Figure 7a shows the climatological mean, vertically integrated mass transport streamfunction for case N13-1. Even for the 15-year mean there are many meanders and small recirculations in the transport streamfunction field. Note that the C-shaped pattern apparent in the surface pressure field does not appear in the streamfunction. The maximum transport in the subtropical gyre is approximately 60 Sv within the tight recirculation northeast of Cape Hatteras. The mean transport between Cuba and Florida is 22.8 Sv, with 18.2 Sv entering the Caribbean Sea between Hispañola and the South American coast and 4.5 Sv entering through Windward Passage. The mean streamlines entering the Caribbean all cross the 25°N latitude circle in the interior to the east of 55°W, consistent with the scheme of Schmitz and Richardson (1991). The maximum transport in the subpolar gyre is about 30 Sv within the Labrador Sea.

The difference between the model mean transport streamfunction and the streamfunction computed from the Sverdrup relation Eq. (3) using annual mean HR wind is shown in Fig. 7b. East of the Mid-Atlantic Ridge the model transports agree with the Sverdrup transports to within 5 Sv. There are large departures all along the western boundary as expected, but also in the interior of both the subtropical and subpolar gyres. In the subtropical gyre, the model predicts stronger anticyclonic circulations to the south of the Gulf Stream and in the Newfoundland Basin. Over much of the subpolar gyre, the model predicts a less intense cyclonic circulation than would be expected from Sverdrup balance.

To provide a more quantitative comparison, profiles of the mean transport streamfunction along 25°N for each of the cases, along with the transports predicted by Sverdrup balance, are shown in Fig. 8 (note that the sign of the streamfunction has been changed from that used in Fig. 7 in order to allow direct comparison with Fig. 1). For each case, the departures from Sver-

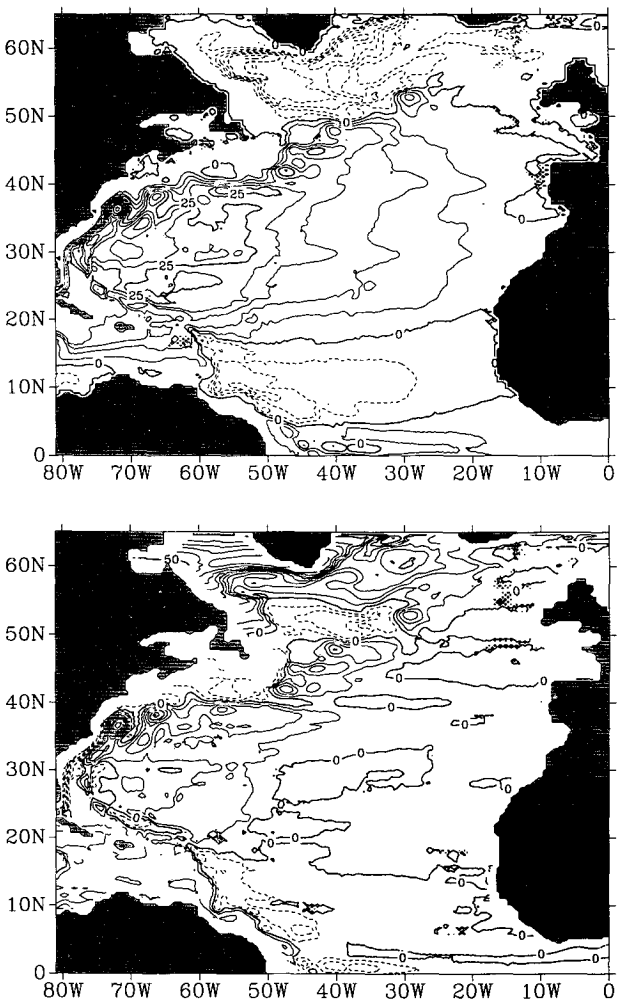

FIG. 7. (a) Climatological-mean barotropic transport streamfunction for case N13-1. Contour interval is 5 Sv. (b) Difference between the model climatological-mean barotropic transport streamfunction and the streamfunction for the Sverdrup transport computed from Eq. (3) using annual mean Hellerman–Rosenstein winds. Contour interval is 5 Sv.

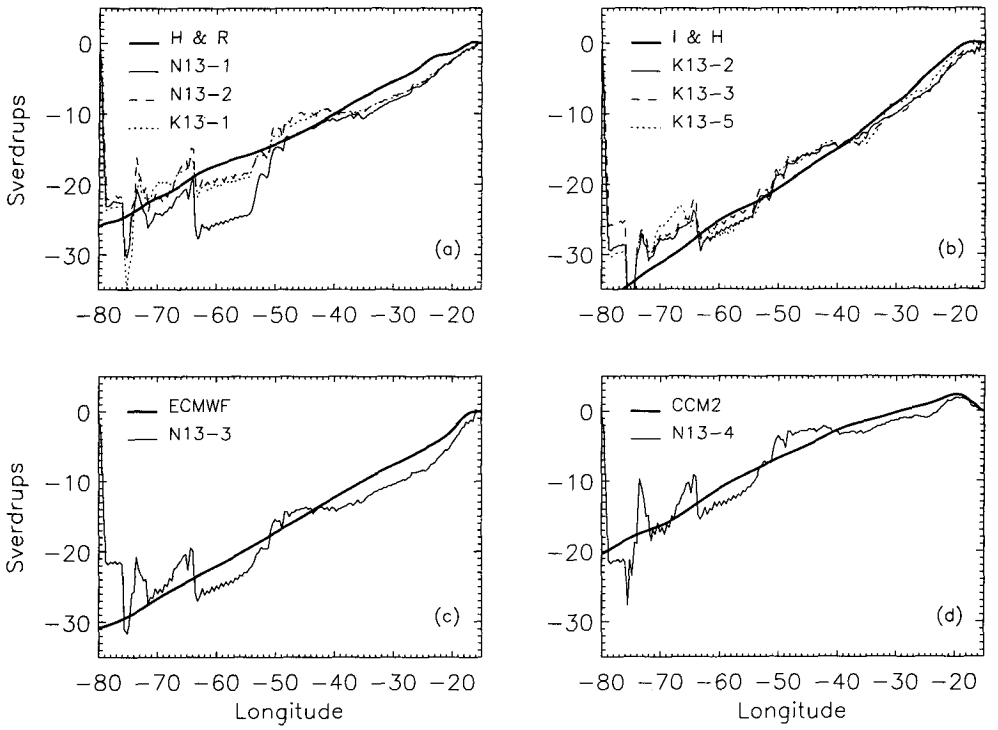

FIG. 8. Vertically integrated transport as a function of longitude at 25°N. (a) Cases forced with HR winds. (b) Cases forced with IH winds. (c) Case forced with ECMWF winds. (d) Case forced with CCM2 winds.

drup balance accumulate in such a way that the model agrees quite well with the Sverdrup prediction at the edge of the western boundary current near 70°W, while the differences between cases can be as large as 10 Sv. There are significant local deviations from Sverdrup balance in the vicinity of the Mid-Atlantic Ridge and near the Bermuda Rise, as well as in the western boundary current. The enhanced southward transport centered on 52°W is associated with the current following the western flank of the Mid-Atlantic Ridge seen in Figs. 4–5. The strong northward transports at 64°W and 73°W are associated with the northward flow of AABW, the former to the east of the Bermuda rise, and the latter along the base of the continental rise. The strong southward transport centered at 74°W is southward flowing NADW. Finally, we identify the two westernmost segments of northward transport with the Antilles Current and the Florida Current. Comparing cases K13-1 and N13-1 we see that the vertically integrated transport is somewhat sensitive to the value of the vertical viscosity. The solutions away from the western boundary appear to be relatively insensitive to the value of the horizontal viscosity, however (comparing K13-2 and K13-3). The differences between cases due to changes in internal parameters are generally less than those due to changes in the wind stress. For cases that are parametrically identical, for example, N13-2, N13-3, and N13-4, the deviations from Sverdrup balance are very similar; that is, the departures are independent of the wind stress forcing itself. Thus, we see that at 25°N deviations of the climatological-mean circulation from Sverdrup balance are largely attributable to the thermohaline-driven bottom flows that are nearly invariant between these cases, and need not be attributed to low-frequency variability or higher-order dynamical effects.

Along 35°N (Fig. 9) the agreement with Sverdrup balance is still quite good in the eastern basin. In all cases the transport is enhanced over the Sverdrup value west of 45°W, possibly associated with the inertial recirculation regime of the Gulf Stream. Along 55°N (Fig. 10), there is generally poor agreement between the model transport and the Sverdrup transport over the entire basin. There is a close correspondence between model cases, however, even though there are quite large differences between the transports implied by Sverdrup balance. At both 35°N and 55°N the sensitivity to both wind stress changes and parameter changes is reduced relative to that at 25°N.

A point of concern when comparing the model results to observation, or when making comparisons of synoptic geostrophic transports and predictions based on climatological wind stress values similar to that in Fig. 1, is that of time variability in the circulation. The comparisons discussed above were based on the climatological mean of the model solutions. Comparisons between the annual-mean circulation for any particular year and the climatological-mean Sverdrup transport

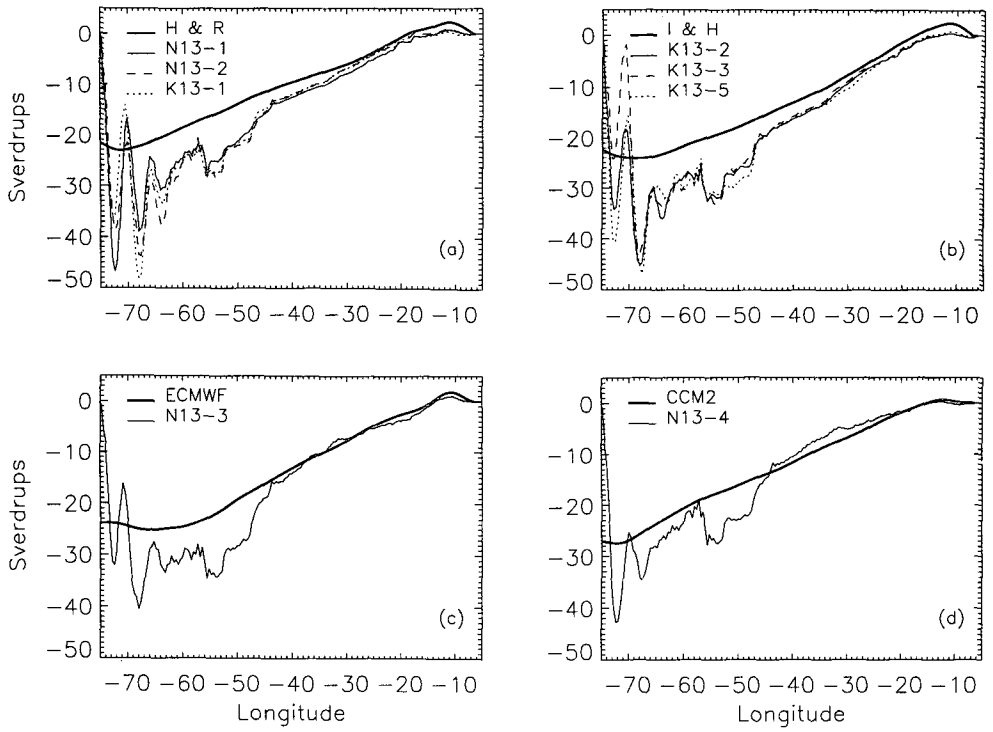

FIG. 9. As in Fig. 8 except at 35°N.

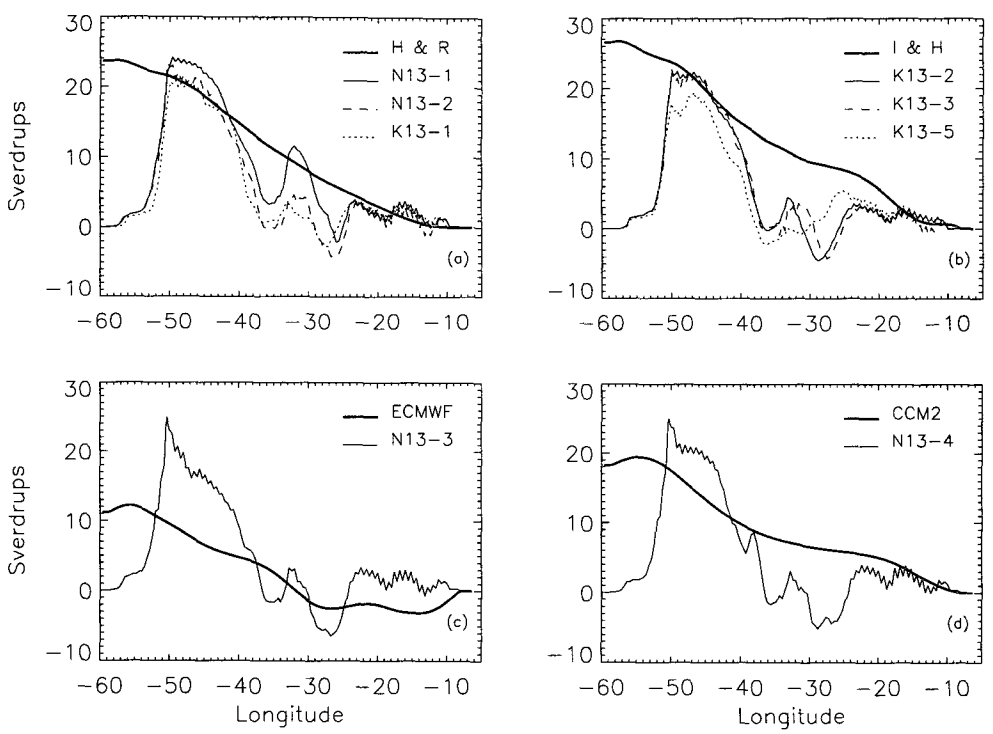

FIG. 10. As in Fig. 8 except at 55°N.

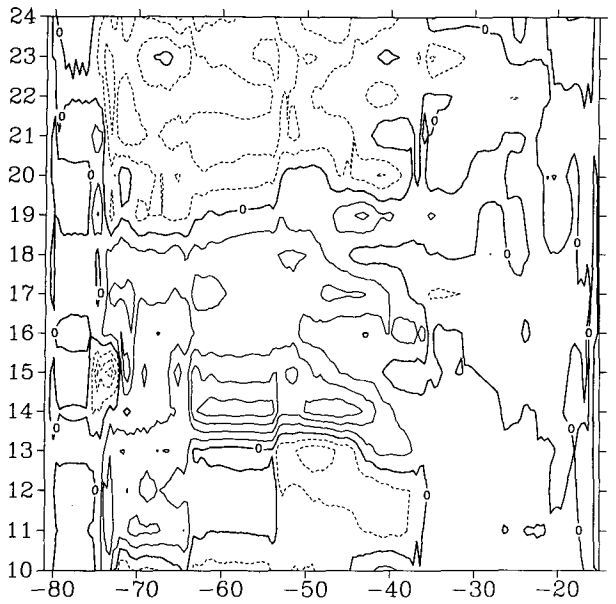

FIG. 11. Annual anomaly (annual mean minus climatological mean) of the barotropic transport streamfunction for case N13-1 along 25°N. Contour interval is 2 Sv. Negative anomalies are dashed.

are much less favorable. In Fig. 11 we plot the annual anomaly (individual annual mean minus the climatological annual mean) of the barotropic transport streamfunction along 25°N for the last 15 years of case N13-1. We see that the variability of the annual means in the western basin is as large as the deviations of the climatological mean from Sverdrup balance. There appear to be long timescale (4–5 year) oscillations in the transport over a broad range of longitudes. The variability is drastically reduced west of the Bahama Banks, however. It also appears that the Bermuda rise at 63°W is effective in blocking some of the interannual variability. At this point it is difficult to say whether these long period oscillations are a residual of the model spinup or are being actively generated by the model through dynamical processes. There does appear to be a signature of zonally elongated propagating bands in the barotropic streamfunction similar to those described by Cox (1987), suggesting active generation. Further analyses of this low-frequency barotropic variability are currently under way. Taking into consideration the previous results of Böning et al. (1991b) concerning seasonal and subseasonal variability, we see that the model solutions contain a rich spectrum of variability even outside the frequency band of the forcing. This presents some difficulty in drawing robust conclusions about model sensitivity even when considering means over 5-year periods.

5. Meridional mass transport at 25°N

To provide further quantitative decomposition of the transport at 25°N we show for selected cases (Fig. 12) the meridional transport across areas defining the Florida Current, the upper, deep, and bottom layers of the western boundary current system, and the surface and deep interior. The cases chosen are the standard HR forcing case, the CCM2 case, which has the smallest Sverdrup transport, and the standard IH case, which has the largest Sverdrup transport. The choice of 71.4°W is arbitrary, but puts the division between the boundary current and the interior to the east of the mean position of the northward flowing AABW on the western boundary. Also, as discussed above, there is generally good agreement between the model predicted climatological-mean barotropic transport and the Sverdrup transport at this longitude. The upper 1000-m meter interior transport, in turn, closely corresponds to the Sverdrup value, as it must in order that net topographic influences be small. In each case there is a

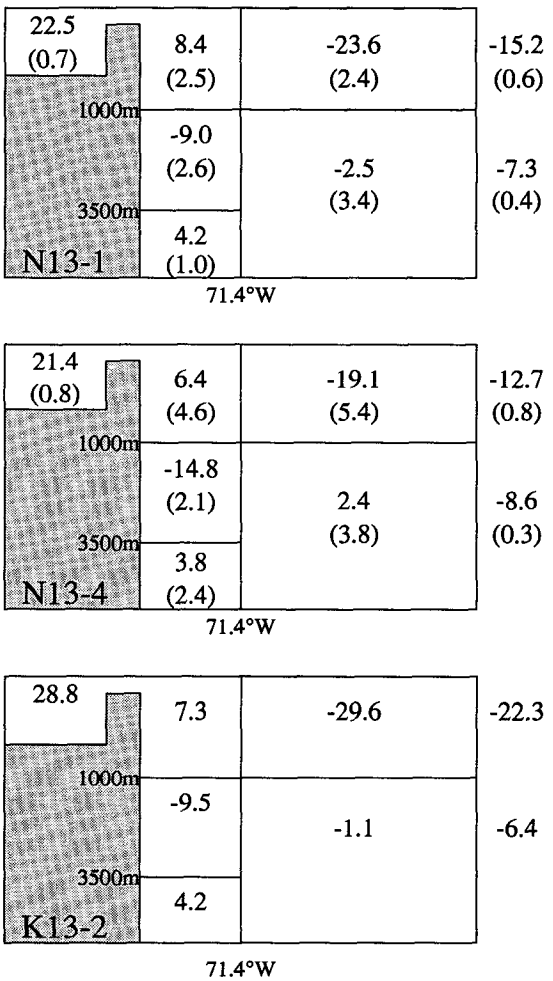

FIG. 12. Mass balance on the 25°N section for cases N13-1, N13-4, and K13-2. Positive values indicate northward transport (Sverdrups). Numbers in parentheses are the standard deviation of the annual means (standard deviations are not available for the K13-n series). Values to the right of the boxes indicate the net transport east of the Bahamas.

TABLE 2. Mean transport in temperature layers for the Florida Current and the Atlantic east of the Bahamas. The model values for case N13-2 were computed from monthly mean climatological velocities and temperatures, and then averaged to form the annual mean. Those for cases K13-1 and K13-2 were computed from climatological annual-mean temperatures and velocities; SR indicates values of Schmitz and Richardson (1991).

	Florida Current				Bahamas–Africa			
Layer	SR	N13-2	K13-1	K13-2	SR	N13-2	K13-1	K13-2
>24	8.1	5.0	6.2	9.7	−1.0	1.7	1.6	2.1
17–24	9.3	10.0	9.2	10.6	−8.5	−11.9	−12.3	−16.8
12–17	6.6	4.3	5.4	5.3	−2.9	−4.7	−5.0	−7.2
7–12	5.0	2.3	2.3	3.0	1.9	−0.4	−0.5	−0.5
<7	0.5	0.0	0.0	0.0	−19.0	−6.5	−7.0	−6.4
Sum	29.5	21.8	23.1	28.8	−29.5	−21.8	−23.1	−28.8

net southward transport of NADW and northward transport of AABW along the western boundary. The deep interior transport is weak, with the variability exceeding the mean, and the sign is variable from case to case. The net transports east of the Bahamas both above and below 1000 m are southward in all cases.

The year to year variability in the transport in the Florida Current is small relative to that in the interior boxes. The enhanced variability east of the Bahamas can be attributed to low-frequency lateral meandering of the western boundary current system resulting in an exchange of transport between the interior and western boundary current boxes. The variability in the net upper and net deep transports east of the Bahamas are small and comparable to those for the Florida Current. The low-frequency variability and the rather short averaging periods for some of the cases make it difficult to draw definitive conclusions about the sensitivity of the division of the transport between the boundary current and interior domains. However, we can make a few conclusions based on those components that have weak year to year variability. For the HR, ECMWF (not shown), and CCM2 cases, if the net deep southward transport of 6.5–8.5 Sv were completely returned through the Caribbean and Straits of Florida, this would leave a partition of the upper wind-driven circulation (as measured by the climatological Sverdrup value) of approximately two-thirds, or 14–15 Sv, passing through the Florida Current and one-third, or 7–8 Sv, passing to the east of the Bahamas. The cases using the IH winds tend to have a larger fraction of the interior Sverdrup transport passing through the Florida Current. The response of the transport in the Straits of Florida to a change in wind stress is thus not consistent across all cases. The Florida Current transport is essentially unchanged from the HR cases to the cases with ECMWF or CCM2 winds. In these cases the adjustment to changes in the interior Sverdrup transport must occur to the east of the Bahamas. The changes in response to the IH winds occur primarily in the Florida Current (the change in the mean is well above the standard deviation), implying little change east of the Bahamas. Further, the net deep southward transport is clearly too weak in all cases. If the thermohaline circulation were increased by 7–10 Sv, the transport of the Florida Current would be quite close to the observed value for the HR, ECMWF, and CCM2 cases, but too strong for the IH cases.

As a final comparison at the 25°N section we present in Table 2 a decomposition of the transport into potential temperature layers for the Florida Current and the entire basin east of the Bahamas for selected cases. The layers were chosen following Schmitz and Richardson (1991). In the Florida Current the transports for cases driven with HR winds are below the observational estimates for all layers (except a slight excess in the 17°–24°C layer in case N13-2), and the total transport is 6.4–7.8 Sv lower than observed. The increase in Florida Current transport with the change to IH winds occurs primarily in the two warmest layers, bringing the total transport close to the observed value. Schmitz and Richardson associate the transports in the warmest layer and in the 7°–12° layer with water of Southern Hemisphere origin, that is, as components of the thermohaline cell. While the strength of the overturning in the model is clearly deficient, the transport deficit does not occur exclusively in these layers, and the warmest layer is clearly responding to changes in wind stress. The weakness of the model overturning cell is also apparent in the very low southward transport in the coldest layer in the interior. All cases show an enhancement of the southward transport in the 12°–24°C range relative to the Schmitz and Richardson estimate. Böning et al. (1994) and Böning et al. (1995) address this deficiency in the model thermohaline transport, and its sensitivity to resolution, and a variety of forcing and parameterization specifications.

6. Does the Sverdrup relation account for the mid-Atlantic circulation?

As mentioned above, several studies have attempted to determine whether the Sverdrup relation can account for the estimated transport at midlatitudes in the

North Atlantic. In this section we diagnose the terms in the linear, vertically integrated, vorticity equation (1) from the mean state of case N13-2 in order to address this question directly. The vertical velocity at the bottom, w_b, is estimated as the vertical velocity at the top of the bottom grid cell at each point. (We use the velocity at the center of the scalar grid cells; the model also computes a separate vertical velocity for grid cells centered on velocity points.) The vertical velocity at the surface, w_s, is taken as the vertical velocity at the bottom of the first model level. The vertically integrated meridional transport used here is the total transport, not just the geostrophic component. As is well known, the vertical velocity field in the Bryan–Cox model tends to be rather noisy, and this is the case for the present implementation. For purposes of illustration we have smoothed each field using a simple 7 point $\times$ 7 point box car filter.

Away from the boundary, the surface pumping corresponds very closely to the Ekman pumping, or wind stress curl distribution. Within the subtropical gyre, the major patterns in the bottom velocity field can be identified with the topographically trapped currents described in sections 3 and 4. The terms are plotted along the same zonal sections as used above in the discussion of the transport. At 25°N (Fig. 13, top), we see that a balance between surface pumping and planetary vorticity advection exist only within the limited ranges of longitudes of approximately 25°–35°W and 55°–63°W. Linear vorticity dynamics, including the bottom torque, does provide a first-order description of the dynamics to within a few degrees of the western boundary, however. At 35°N (Fig. 13, middle), linear dynamics explains the vorticity balance over the basin east of 50°W except near 20°W. In the western basin there are large-scale meanders in the mean Gulf Stream where higher-order dynamics apply. At 55°N (Fig. 13, bottom), there is essentially no relationship between the meridional transport and the Ekman pumping terms. The bottom velocity is seen to agree in sign with the meridional transport in the core of the North Atlantic Current between 35° and 40°W, and near 25°W, but the quantitative correspondence is poor.

7. Conclusions

The goals of this study are severalfold. First, we wish to establish the ability of the model to reproduce the climatological-mean circulation of the North Atlantic by comparing key aspects of the solution with recently proposed circulation schemes. This is meant to complement previous CME studies with more regional or process orientations. Second, we have used the model solution to evaluate the degree to which simple dynamical models of the circulation are able to describe the large-scale mass transport in midlatitudes. Third, we have examined the model solution for several wind stress climatologies, helping both to determine the sensitivity of the model to the specification of its forcing, and to test the reliability of the climatologies themselves.

The one-third degree version of the CME North Atlantic model is able to capture many of the features of the climatological mean, midlatitude circulation as defined, for example, by the recent synthesis of Schmitz and McCartney (1993). There are a number of important discrepancies, however. The Gulf Stream separates from the coast north of Cape Hatteras, and the model lacks a cyclonic recirculation gyre west of the Grand Banks. These two problems are quite likely related to one another, based on the recent study of Ezer and Mellor (1992) examining the sensitivity of Gulf Stream separation to various forcing mechanisms in a regional model. In the full basin model it is more difficult to establish cause and effect, however. The core of the southward flowing North Atlantic Deep Water occurs at too shallow a depth and too warm a temperature. The strength of the meridional overturning circulation and contribution of waters of Southern Hemisphere origin to the transport across 25°N are too low by 7–10 Sv. The weakness of the thermohaline circulation accounts for a similar deficit in the transport through the Straits of Florida and to a poleward heat transport that is approximately 30% lower than observations suggest. As described in Böning et al. (1995), the deficit of the southward transport of NADW at 25°N is primarily due to loss through upwelling near the western boundary between 30° and 40°N rather than to insufficient deep-water formation. The reader is referred to that paper for a more complete discussion of this problem and its dependence on model parameters and resolution.

By comparing the model's vertically integrated transport to the Sverdrup transport and by examining the terms in the linear vorticity balance, we see that the wind forcing is the primary mechanism controlling the large-scale circulation in the eastern subtropical gyre. At 25°N, thermohaline driven bottom flows may cause strong local departures from the Sverdrup solution, but these nearly integrate to zero across the basin. While the net southward transport in the interior of the basin differs by more than 10 Sv between the strongest and weakest circulation cases, in each case there is good agreement between the Sverdrup prediction and the model transport at the outer edge of the western boundary current system. We need to consider this result with some caution, however, in light of inaccuracies in the deep thermohaline-driven currents as described above. An enhanced circulation of North Atlantic Deep Water may induce stronger bottom torques, though they would probably be confined to the western boundary region. The model does seem to represent the circulation of AABW reasonably well. The strongest bottom torques away from the western boundary are associated with the circulation of this water mass, so the vertically integrated vorticity balance

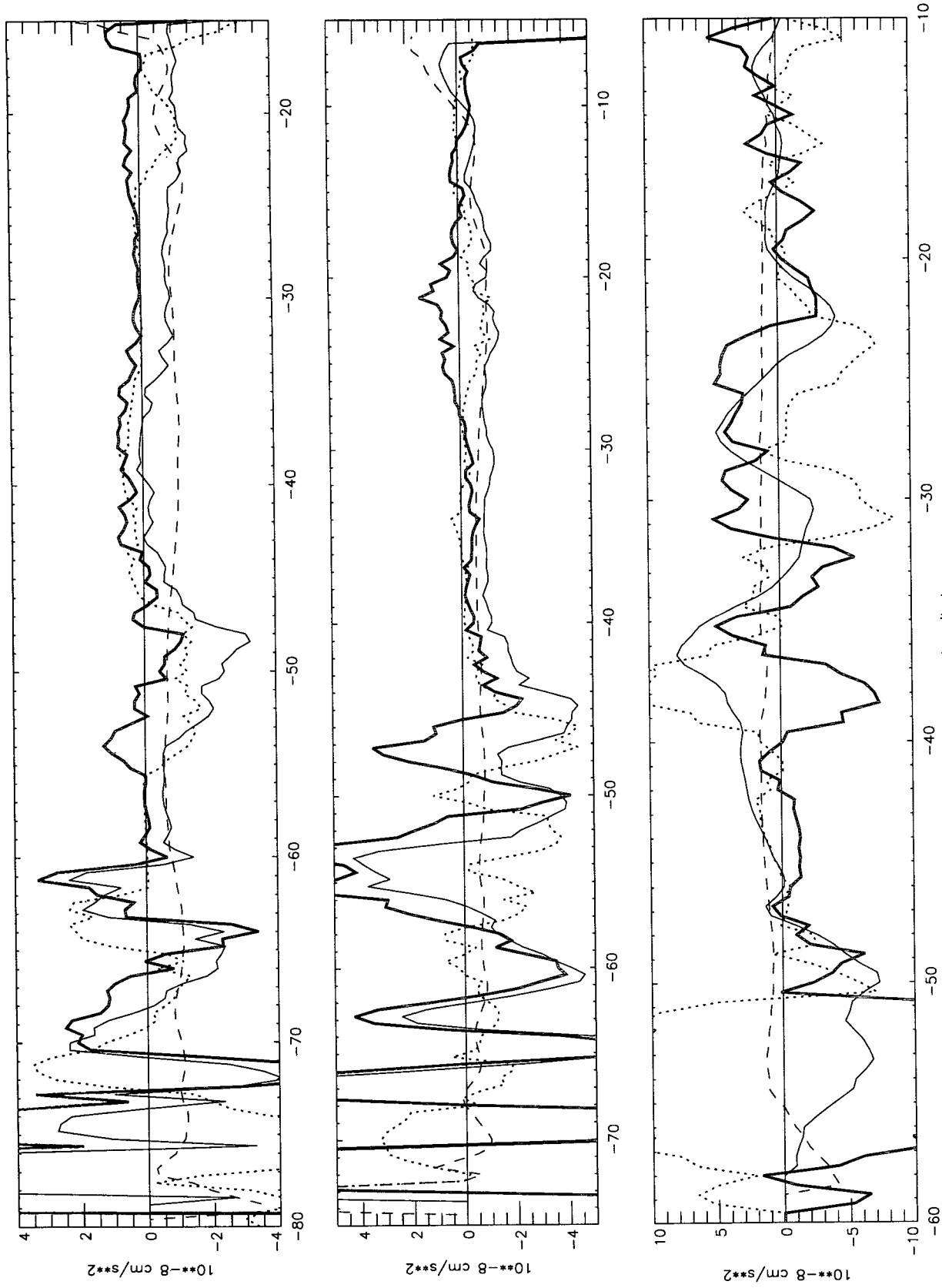

FIG. 13. Climatological mean terms in the linear vorticity equation (1) for case N13-1. Planetary vorticity advection βV (solid), Ekman pumping fw_s (dashed), bottom torque—fw_b (dotted), residual $\beta V - fw_s + fw_b$ (thick solid): (top) along 25°N, (middle) along 35°N, and (bottom) along 55°N.

may be relatively unaffected by changes in the circulation of NADW. Experiments with modified northern boundary conditions to enhance the inflow of NADW are currently under way to help resolve this question. In summary, that Sverdrup balance provides a good estimate of the basin-integrated meridional transport is more a coincidence of the particular configuration of the deep flows at 25°N than a validation of the underlying assumptions of negligible influence of bottom topography.

In the northwestern portion of the subtropical gyre, in the vicinity of the Gulf Stream, higher-order dynamics become important and linear vorticity dynamics is unable to explain the model vertically integrated transport. In the subpolar gyre the solutions bear essentially no resemblance to the Sverdrup transport. Further, there is little change in the vertically integrated transport between cases, despite large changes in the Sverdrup transport implied by the different wind stress climatologies. Linear vorticity dynamics, including the effects of bottom torques, cannot explain the distribution of horizontal mass transport within the subpolar gyre.

The results of this study have several implications for our ability to observe the mean, large-scale circulation in the North Atlantic and for using models to validate estimates of the distribution of wind stress. First, we find very low frequency variations in the barotropic transport in the western subtropical basin that result in lateral meandering of the boundary current system. At 25°N the annual anomalies of the transport are up to 50% of the climatological mean value. The variability is greatly reduced west of the Bahamas, however. This suggests that direct estimates of the mean transport of the Florida Current based on records of a few years duration should be fairly robust. Direct measurements of the climatological mean transport of the western boundary current system east of the Bahamas will be much more difficult, however. This is already apparent in the estimates from multiyear deployments of current meters in this region. There is some inconsistency in the adjustment of the western boundary current system to changes in the wind stress distribution between cases. The change from the Hellerman and Rosenstein wind stress to the ECMWF or NCAR CCM2 wind stresses resulted primarily in a change in the boundary current transport east of the Bahamas with little change in the transport of the Florida Current. The change to the Isemer and Hasse wind stress estimate, on the other hand, resulted in a large change in the transport of the Florida Current. This suggests that measurements of the transport in the Straits of Florida alone will not provide a strong constraint on estimates of the wind stress distribution. Combined with the large year-to-year variability in the boundary current transports east of the Bahamas, calibrating wind stress estimates through direct measurements of ocean transport will be difficult. Second, bottom torques are of comparable magnitude to Ekman pumping in the vorticity budget over most of the basin. This makes it difficult to justify the use of Sverdrup balance in any diagnostic circulation scheme. The result that Sverdrup balance holds in a basin-integrated sense at 25°N may be only a coincidence of the particular deep circulation pattern predicted by the model, as discussed above. If this result proves robust to further changes in the model, however, it should prove to be an effective constraint that can be used in combining hydrographic measurements, current meter measurements, and wind stress estimates into quantitative budgets for mass, heat, or other tracers for the North Atlantic.

Acknowledgments. We would like to thank R. Budich, R. Döscher, and P. Herrmann at Kiel, and J. Chow and K. Holcomb at NCAR for their assistance in the model integrations and analysis.

REFERENCES

Anderson, D. L. T., and P. D. Killworth, 1977: Spin-up of a stratified ocean with topography. *Deep-Sea Res.*, **24**, 709–732.

——, K. Bryan, A. E. Gill, and R. C. Pacanowski, 1979: The transient response of the North Atlantic: Some model studies. *J. Geophys. Res.*, **84**, 4795–4815.

Beckman, A., C. W. Böning, C. Köberle, and J. Willebrand, 1994: Effects of increased horizontal resolution in a simulation of the North Atlantic Ocean. *J. Phys. Oceanogr.*, **24**, 326–344.

Böning, C. W., R. Döscher, and H.-J. Isemer, 1991a: Monthly mean wind stress and Sverdrup transports in the North Atlantic: A comparison of the Hellerman–Rosenstein and Isemer–Hasse climatologies. *J. Phys. Oceanogr.*, **21**, 221–235.

——, and ——, and R. G. Budich, 1991b: Seasonal transport variation in the western subtropical North Atlantic: Experiments with an eddy resolving model. *J. Phys. Oceanogr.*, **21**, 1271–1289.

——, F. O. Bryan, W. R. Holland, and R. Dösher, 1994: Thermohaline circulation and poleward heat transport in a high-resolution model of the North Atlantic. *J. Phys Oceanogr.*, submitted.

——, W. R. Holland, F. O. Bryan, G. Danabasoglu, and J. C. McWilliams, 1995: An overlooked problem in model simulations of the thermohaline circulation and heat transport in the Atlantic Ocean. *J. Climate*, **7**, in press.

Bryan, F., and W. R. Holland, 1989: A high resolution simulation of the wind- and thermohaline-driven circulation in the North Atlantic Ocean. *'Aha Huliko'a Parameterization of Small-Scale Processes*, P. Muller and D. Henderson, Eds., Hawaii Institute of Geophysics, 99–115.

——, I. Wainer, and W. R. Holland, 1994: Sensitivity of the tropical Atlantic circulation to specification of wind stress climatology. *J. Geophys. Res.*, submitted.

Bryan, K., 1969: A numerical method for the study of the circulation of the world ocean. *J. Comput. Phys.*, **4**, 347–376.

Bunker, A. F., 1976: Computations of surface energy flux and annual air–sea interaction cycles of the North Atlantic Ocean. *Mon. Wea. Rev.*, **104**, 1122–1140.

Cox, M. D., 1984: A primitive equation three dimensional model of the ocean. GFDL Ocean Group Tech. Rep. No. 1, Geophysical Fluid Dynamics Laboratory/NOAA, 56 pp.

——, 1987: An eddy-resolving model of the ventilated thermocline: Time-dependence. *J. Phys. Oceanogr.*, **17**, 1044–1056.

Ezer, T., and G. L. Mellor, 1992: A numerical study of the variability and separation of the Gulf Stream, induced by surface atmo-

spheric forcing and lateral boundary flows. *J. Phys. Oceanogr.*, **22,** 660–682.

Hack, J. J., B. A. Boville, B. P. Briegleb, J. T. Kiehl, P. J. Rasch, and D. L. Williamson, 1993: Description of the NCAR Community Climate Model (CCM2). NCAR/TN-382 + STR, National Center for Atmospheric Research, Boulder, CO, 108 pp.

Hall, M., and H. Bryden, 1982: Direct estimates and mechanisms of ocean heat transport. *Deep-Sea Res.*, **29,** 339–359.

Han, Y.-J., 1984: A numerical world ocean general circulation model. Part II: A baroclinic experiment. *Dyn. Atmos. Oceans,* **8,** 141–172.

Harrison, D. E., 1989: On climatological monthly mean wind stress and wind stress curl fields over the world ocean. *J. Climate,* **2,** 57–70.

Hellerman, S., and M. Rosenstein, 1983: Normal monthly wind stress over the world ocean with error estimates. *J. Phys. Oceanogr.*, **13,** 1093–1104.

Holland, W. R., 1973: Baroclinic and topographic influences on the transport in western boundary currents. *Geophys. Fluid Dyn.*, **4,** 187–210.

Isemer, H.-J., and L. Hasse, 1987: *The Bunker Climate Atlas of the North Atlantic Ocean.* Vol. 2: *Air–Sea Interactions,* Springer-Verlag, 218 pp.

Large, W. G., and S. Pond, 1981: Open ocean momentum flux measurements in moderate to strong winds. *J. Phys. Oceanogr.*, **11,** 324–336.

Larsen, J. C., 1992: Transport and heat flux of the Florida Current at 27°N derived from cross-stream voltages and profiling data: Theory and observations. *Philos. Trans. Roy. Soc. London A,* **338,** 169–236.

Leaman, K. D., and J. E. Harris, 1990: On the average absolute transport of the Deep Western Boundary Current east of Abaco Island, Bahamas. *J. Phys. Oceanogr.*, **20,** 467–475.

Lee, T. N., W. Johns, F. Schott, and R. Zantopp, 1990: Western boundary current structure and variability east of Abaco, Bahamas at 26.5°N. *J. Phys. Oceanogr.*, **20,** 446–466.

Leetmaa, A., P. Niiler, and H. Stommel, 1977: Does the Sverdrup relation account for the mid-Atlantic circulation? *J. Mar. Res.*, **35,** 1–10.

Levitus, S., 1982: *Climatological Atlas of the World Ocean.* NOAA Prof. Paper 13, U.S. Govt. Printing Office, 173 pp.

Olson, D. B., F. A. Schott, R. J. Zantopp, and K. D. Leaman, 1984: The mean circulation east of the Bahamas as determined from a recent measurement program and historical XBT data. *J. Phys. Oceanogr.*, **14,** 1470–1487.

Roemmich, D., 1980: Estimation of meridional heat flux in the North Atlantic by inverse methods. *J. Phys. Oceanogr.*, **10,** 1972–1983.

——, and C. Wunsch, 1985: Two transatlantic sections: Meridional circulation and heat flux in the subtropical North Atlantic Ocean. *Deep-Sea Res.*, **32,** 619–664.

Schmitz, W. J., Jr., and P. L. Richardson, 1991: On the sources of the Florida Current. *Deep-Sea Res.*, **38**(Suppl. 1), 389–409.

——, and M. S. McCartney, 1993: On the North Atlantic circulation. *Rev. Geophys.*, **31,** 29–49.

——, J. D. Thompson, and J. R. Luyten, 1992: The Sverdrup circulation for the Atlantic along 24°N. *J. Geophys. Res.*, **97,** 7251–7256.

Schott, F. A., and C. W. Böning, 1991: Evaluation of the WOCE model in the western equatorial Atlantic: Upper-layer circulation. *J. Geophys. Res.*, **96,** 6993–7004.

Spall, M. A., 1990: Circulation in the Canary Basin: A model/data analysis. *J. Geophys. Res.*, **95,** 9611–9628.

——, 1992: Rossby wave radiation in the Cape Verde frontal zone. *J. Phys. Oceanogr.*, **22,** 796–807.

Stammer, D., and C. W. Böning, 1992: Mesoscale variability in the Atlantic Ocean from Geosat altimetry and WOCE high-resolution numerical modeling. *J. Phys. Oceanogr.*, **22,** 732–752.

Stramma, L., 1984: Geostrophic transport in the warm water sphere of the eastern subtropical North Atlantic. *J. Mar. Res.*, **42,** 537–558.

Treguier, A.-M., 1992: Kinetic energy analysis of an eddy resolving primitive equation model of the North Atlantic. *J. Geophys. Res.*, **97,** 687–701.

Trenberth, K. E., W. G. Large, and J. G. Olson, 1990: The mean annual cycle in global wind stress. *J. Phys. Oceanogr.*, **20,** 1742–1760.

Wunsch, C., and D. Roemmich, 1985: Is the North Atlantic in Sverdrup balance? *J. Phys. Oceanogr.*, **15,** 1876–1880.